

Vigna stipulacea mediated Fe nanoparticles synthesis: a greener approach for sequestration of Pb²⁺ from aqueous environment

Mafaz Ahamed R.^{1*} and Saraswathi R.²

¹*Department of Civil Engineering, Velammal College of Engineering and Technology, Madurai-625009, Tamil Nadu, India

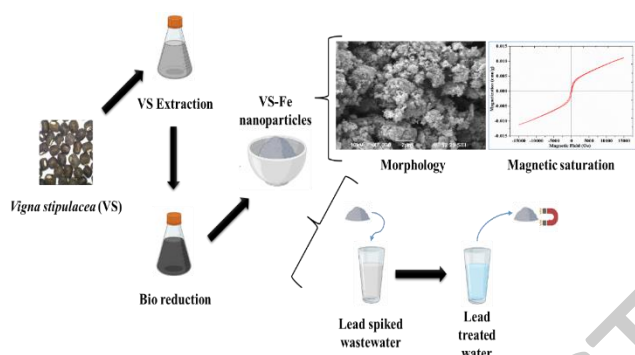
²Department of Civil Engineering, Coimbatore Institute of Technology, Coimbatore-641014, Tamil Nadu, India

Received: 08/05/2023, Accepted: 13/11/2023, Available online: 20/11/2023

*to whom all correspondence should be addressed: e-mail: mafaz.anwari@gmail.com

<https://doi.org/10.30955/gnj.005132>

Graphical abstract



Abstract

The greener approach offers a viable, sustainable and eco-friendly way to synthesize nanoparticles. This study used the seed extract of *Vigna stipulacea* (VS) as a bio-reducing agent to synthesize iron nanoparticles (VS-Fe). The VS seed extract contains polyphenols and lignin content that acted as a bio-reducing agent during VS-Fe formation. The *Vigna stipulacea*-mediated Fe nanoparticles were characterized using UV, XRD, FTIR, EDAX and BET surface analysis. The as-synthesized VS-Fe, comprised of Fe⁰ phase and Fe hydroxides, had an average crystallite size of 30.65 nm. It possessed a surface area of 199.189 m²/g and magnetic saturation of 11.21 m emu. The VS-Fe exhibited excellent adsorptive behavior during the sequestration of Pb²⁺ ions from an aqueous environment. The Pb²⁺ uptake was maximum (96.7%) under the optimal conditions of 60 min contact time, 0.01 g/ 100 mL VS-Fe dosage and pH 6. The equilibrium data of Pb²⁺ adsorption was more appropriate with pseudo-second-order kinetics (R² = 0.9903) and Langmuir isotherm (R² = 0.9941) with q_{max} of 1020.50 mg/g. Thus, the dominance of chemisorption in Pb²⁺ removal was revealed. It was further confirmed with the SEM micrograph of Pb-loaded VS-Fe nanoparticles. Overall, this study demonstrated the inexpensive and non-toxic way of synthesizing Fe nanoparticles and their utilization in effectively removing Pb²⁺ ions from water.

Keywords: Fe nanoparticles, green synthesis, polyphenol, lead removal, *Vigna stipulacea*.

1. Introduction

The preservation of water quality has become a global concern owing to the synchronization of rapid industrialization with the disposal of an enormous quantity of wastewater into the aquatic environment (Thanh *et al.* 2018). Most industrial effluents are rich in heavy metals, including lead which is toxic and non-biodegradable and bioaccumulates in living cells, causing severe health issues in humans and animals (Kaur *et al.* 2018; Ali *et al.* 2019). Lead is commonly used in electroplating, battery manufacturing and metal processing industries. In humans, lead can cause infertility, asthma and renal abnormalities, whereas its exposure leads to bioaccumulation in bones, teeth and kidneys (Thirulogachandar *et al.* 2014; Araujo *et al.* 2018). A growing concern emphasizes the requirement for an efficient treatment for lead removal before they are released into the aquatic environment. Traditional heavy metal removal methods include oxidation-precipitation, ion exchange (Dong *et al.* 2019), coagulation-electrocoagulation (El-Hosiny *et al.* 2018), adsorption (Lin *et al.* 2020; Nithyalakshmi *et al.* 2023), photocatalytic degradation (Dayanidhi *et al.* 2020), and membrane filtration (Ding *et al.* 2020). Identifying an effective technique for this purpose is challenging, primarily due to the cost implications and potential environmental toxicity associated with the resulting by-products. Adsorption remains a prominent technique due to its uncomplicated design, extensive adaptability, economical nature, high efficacy, ease of use, absence of secondary pollutant generation, and viability at low concentrations (Jayalakshmi and Jeyanthi, 2019). Several adsorbents, including biopolymers, fly ash, and activated carbon, are efficacious in mitigating heavy metals in aqueous solutions. However, some of their use has been constrained by considerations like their high cost, difficulties in separation, strong reaction conditions, and toxicity (Yurekli, 2016).

The utilization of nanoparticles to eliminate various pollutants present in an aqueous environment has routed to the significant development of novel techniques in metal removal/recovery from water. The application of these particles is mainly due to their large surface area, high

surface energy and high reaction rate (Balasubramanian *et al.* 2021). Recently, there has been ongoing research on the synthesis of nano adsorbents utilizing plant intermediates, which has been recognized as a viable and effective approach. The process of synthesizing nanoparticles through plant mediation involves the utilization of environmentally friendly biomolecules that serve as both reducing and capping agents. These biomolecules are non-toxic and biodegradable, and their use helps minimize the synthesized nanoparticles' oxidation and agglomeration (Ebrahiminezhad *et al.* 2018; Raman *et al.* 2021). The high cellulose content in plants is responsible for their reducing properties towards heavy metals. The feasibility of utilizing the compound for wastewater treatment is attributed to the existence of functional groups, namely hydroxyl, phenol, and carboxyl (Mohamed *et al.* 2019).

During the last decade, several studies have indicated that Fe nanoparticles effectively address heavy metal pollution, making them a promising solution for treating wastewater polluted with various heavy metals. Moreover, their remarkable attributes and versatile utilities prompted us to opt for the plant extract approach in their production (Lin *et al.* 2020). For instance, the study conducted by Guo *et al.* (2017) reported the utilization of *Euphorbia cochinchensis* leaf extract for the green synthesis of Fe nanoparticles. The synthesized Fe nanoparticles were employed for degrading 2,4-dichlorophenol. Similarly, in a study by Huang *et al.* (2014), Fe nanoparticles synthesized using Oolong tea extract were effectively utilized to degrade malachite green. The Fe nanoparticles were produced in an environmentally friendly manner, resulting in a green synthesis process.

The *Vigna stipulacea* is commonly known as Minni payaru, which is traditionally utilized as animal fodder and green manure in the regions of Southern India. It is a creeping plant and wild species resistant to pests and diseases. It is widely distributed and can be cultivated in open or light-shady lands. However, the information on the phenolic content and antioxidant property of *Vigna stipulacea* is not reported elsewhere due to its close resemblance with *Vigna trilobata* (Harouna *et al.* 2018; Panzeri *et al.* 2022). This study attempts to utilize the seed extract of *Vigna stipulacea* as a bioreducing agent for Fe nanoparticle formation. To date, the literature has not provided significant information regarding the adsorptive behavior of VS-Fe in removing heavy metals. These *Vigna stipulacea* plants are easily domesticated as they require minimal water and demand little care and maintenance. Moreover, the reported VS-Fe nanoparticles showed higher surface and magnetic saturation when compared to other Fe nanoparticles synthesized using various plant extracts (Mandal *et al.* 2020; Saleh *et al.* 2021). In addition, it also showed better adsorption capacity for Pb^{2+} removal with no other functional groups tailored to it (Liu *et al.* 2019; Shi *et al.* 2023).

The main objectives of the study are as follows: (a) synthesizing the Fe nanoparticles through a greener approach using *Vigna stipulacea* as a bioreducing agent ($FeCl_2$ - metal precursor; NaOH - pH stabilizer); (b)

characterizing the synthesized *Vigna stipulacea*-mediated Fe nanoparticles (VS-Fe) to detect their successful formation (UV, XRD, FTIR, VSM, BET, SEM and EDAX); (c) utilizing VS-Fe for eliminating Pb^{2+} ions from water; (d) optimizing the environmental conditions for the effective removal of Pb^{2+} ions using VS-Fe (dosage, pH, contact time, concentration); (d) validating the experimental data of Pb^{2+} adsorption onto VS-Fe through non-linear regression approach (Isotherm and Kinetic modeling).

2. Experimental section

2.1. Materials

The seeds of *Vigna stipulacea* (Minni Payaru) were collected from the local cattle farm in Sivagangai, Tamilnadu, India. The seed extract is used as a reducing agent for the green synthesis of VS-Fe nanoparticles. The chemicals (Merck India, AG) such as Ferrous chloride ($FeCl_2 \cdot 4H_2O$), Sodium hydroxide (NaOH), Ethanol (C_2H_5OH), Sodium nitrate ($NaNO_3$), Hydrochloric acid (HCl), Sulphuric acid (H_2SO_4), Ethanol (C_2H_5OH), Lead nitrate ($Pb(NO_3)_2$) (lead source), tannic acid, acetic acid and alkali lignin were used in this study. Double distilled water is used for preparing all the reagents.

2.2. Preparation of *Vigna stipulacea* seed extract

The *Vigna stipulacea* (VS) seed extract was prepared using the solvent extraction method. The collected *Vigna stipulacea* seeds were initially washed with double distilled water until the dirt/dust in it was removed and oven-dried (Genuine equipments, Hot air oven) for 15 min. Then, the VS seed extract was prepared using a Soxhlet apparatus (250 mL) as follows: The VS seeds (6g) were taken in a cloth bag and placed in the thimble region and double distilled water (100 mL) was used as a solvent. Then, the Soxhlet apparatus was operated under $80^\circ C$ for 4 hr. The VS seed extract was collected in the round-bottomed flask. Then, the contents were filtered using Whatman filter paper (Garde 40). Thus, VS seed extract, free of microparticles (Figure 1), was obtained, transferred to an air-tight container, and preserved in a refrigerator for future use.

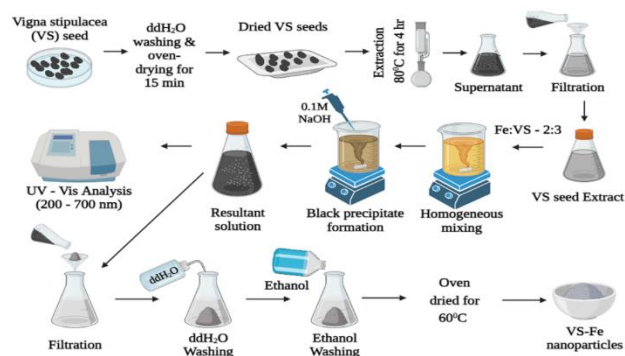


Figure 1. Synthesis of *Vigna stipulacea* - mediated Fe nanoparticles

2.3. Green synthesis of VS-Fe nanoparticles

The schematic diagram of VS-Fe synthesis is depicted in Figure 1. The metal solution of 0.1 M ferrous chloride is prepared using double distilled water. The VS seed extract is added to the metal solution in a 2:3 ratio. The reaction mixture was homogenized using a magnetic stirrer (REMI

2MLH) and the stirring was continued for 1 hr. The reaction mixture's pH was adjusted to 6 using 0.1 M NaOH. A change of colour from yellow to black was visualized, which indicated the VS-Fe nanoparticles formation. Subsequently, the formation of VS-Fe nanoparticles was further confirmed by measuring the absorbance of the resultant solution using a UV-Visible spectrophotometer (Cyberlab). The resultant solution was transferred to a quartz cuvette and the absorbance was measured in the 200 – 700 nm wavelength range. Maximum absorbance was detected at 285 nm (Figure 2(a)), which is the characteristic peak of Fe⁰ formation due to surface plasma resonance (Pan *et al.* 2020; Sivakami *et al.* 2020). The findings from the UV analysis revealed the formation of zero-valent iron nanoparticles using VS seed extract as a reducing agent. The black precipitate was separated by filtering the resultant solution to obtain the VS-Fe nanoparticles formed and the residual solution was decanted. Then it was subsequently rinsed with double distilled water and ethanol to eliminate the residual impurities. Finally, it was desiccated at 60°C using a hot air oven to remove the moisture. The VS-Fe nanoparticles thus obtained were kept in the dark place for future use.

2.4. Instrumentation

The Empyrean X-ray diffractometer (Malvern Panalytical), which operates with a high-power radioactive source (Cu K α , $\lambda = 1.54 \text{ \AA}$), was used to detect the phase formation and crystallinity of VS-Fe nanoparticles. The X-ray diffractogram (XRD) for VS-Fe nanoparticles in powder form was generated in 2θ range of 10° to 90° . The CARL ZEISS Scanning Electron Microscope (SEM) coupled with BRUKER Energy Dispersive X-ray Spectroscopy (EDAX) visualized the surface texture and elemental composition of VS-Fe nanoparticles. Their sample preparation included the gold sputtering of VS-Fe nanoparticles. The Shimadzu Fourier Transform Infrared Spectrometer (FTIR) detected the VS-Fe nanoparticles' functional group by measuring their IR spectra under $400 - 4000 \text{ cm}^{-1}$ with 0.5 cm^{-1} resolution. The VS-Fe nanoparticles were homogenously mixed with spectroscopic grade KBr before FTIR analysis. The Quanta Surface Area analyzer measured the surface area characteristics of VS-Fe nanoparticles. The VS-Fe nanoparticles (0.0139 g) were preheated upto 100°C to liberate the water-bound molecules prior to the surface area analysis. The Lakeshore Vibrating Sample Magnetometer (VSM) evaluated the magnetic saturation of VS-Fe nanoparticles. The Toplab (TL-3800AA) Atomic Absorption Spectrometer measured the residual Pb²⁺ concentration after the absorption. The pH of the residual/metal solutions was determined from the Newlabs equipment pH meter.

$$\text{Pb}^{2+} \text{ removal (\%)} = \frac{(C_0 - C_e)}{C_0} * 100$$

(Nithyalakshmi and Saraswathi 2021)

(1)

$$q_e = \frac{(C_0 - C_e) * V}{m}$$

(Patil *et al.* 2022)

(2)

where C_0 (mg/L) (Patil *et al.* 2022), is the initial Pb²⁺ concentration, V (mL) is volume taken, m (g) is VS-Fe

The total polyphenolic composition of VS seed extract was determined using the Folin-Ciocalteu assay, as reported by Khatun and Kim (2021). Initially, the Tannic acid standard solutions (0-500 $\mu\text{g/mL}$) were prepared in methanol for calibration. Then, the methanolic extract of VS seeds was prepared using the Soxhlet apparatus. The 10 μL of these samples were added into individual test tubes and mixed with diluted Folin-Ciocalteu reagent (100 μL) for 3 minutes and 1 mL sodium carbonate (0.7 M) was introduced. Each test tube is enclosed with aluminum foil and the reaction is allowed for 60 min at room temperature and their respective absorbances were measured at 750 nm using a UV-Visible spectrophotometer.

The total lignin composition of VS seed extract was determined using an acetyl bromide assay, as Fang *et al.* (2020) reported. Initially, alkali lignin standard solutions were prepared for calibration. Then, VS seeds (5 mg) were subjected to extraction in ethanol/toluene mixture (1:1). The extraction procedure was continued until no trace of absorbance was observed at 280 nm. Afterward, the VS seed powder was dried and transferred into glass tubes containing 1 mL acetyl bromide and 3 mL acetic acid. The glass tubes were then incubated at 70°C for half an hour. Subsequently, the samples were placed in an ice bath and homogenized with 2 M NaOH (0.9 mL), acetic acid (5 mL) and 7.5 M hydroxylamine hydrochloride (0.1 mL). The final volume was raised upto 10 mL using acetic acid and their absorbance was spectrometrically analysed at 280 nm.

2.5. Adsorption of Pb²⁺ using VS-Fe nanoparticles in batch mode

A 1.607 grams of Pb²⁺ nitrate salts were added to 1000 mL of double distilled water to make a 1000 mg/L Pb²⁺ solution. And then, appropriate dilutions were made to obtain desired concentrations of Pb²⁺ solution for batch experimentation. A 100 mL Pb²⁺ solution of desired concentration was taken in a 250 mL Erlenmeyer flask and a known quantity of VS-Fe nanoparticles was added to it. The flasks were then operated at room temperature at 150 rpm using an orbital shaker (Neolab). Once the equilibrium was achieved, the treated solution was filtered using Whatman filter paper (Grade 42) and tested for residual Pb²⁺ concentration using AAS. The process parameters significantly influencing the Pb²⁺ adsorption onto VS-Fe nanoparticles were assessed in the batch experiments. And they are as follows: VS-Fe dosage (0.01 to 0.10 g), pH (3 to 10), contact time (10 to 180 min) and initial Pb²⁺ concentration (5 to 40 mg/L).

The Eq. (1) and (2) determined the percentage removal (Nithyalakshmi and Saraswathi, 2021) of Pb²⁺ (%) and q_e , the Pb²⁺ quantity adsorbed onto VS-Fe (Patil *et al.* 2022), respectively.

nanoparticles' quantity and C_e (mg/L) (Patil *et al.* 2022) is the equilibrium concentration of Pb²⁺.

2.6. Analysis of best fitness

The experimental data of Pb^{2+} removal using VS-Fe was evaluated using non-regression kinetic and isotherm modeling studies. Among the performed modeling studies, the appropriate best-fit model for Pb^{2+} adsorption onto VS-Fe was validated using correlational coefficient (R^2) and Error function values. The root mean square errors (RMSE), Person's Chi-square (χ^2) and Sum of squares of error (SSE) are the Error function (EF) values used for determining the best-fit model (Jayalakshmi and Jeyanthi 2021).

$$R^2 = 1 - \frac{\sum_{n=1}^n (y_{e,n} - y_{c,n})^2}{\sum_{n=1}^n (y_{e,n} - y_{c,mean})^2} \quad (3)$$

$$RMSE = \sqrt{\frac{1}{n-1} \sum_{n=1}^n (y_{e,n} - y_{c,n})^2} \quad (4)$$

$$\chi^2 = \sum_{n=1}^n \frac{(y_{e,n} - y_{c,n})^2}{y_{e,n}} \quad (5)$$

$$SSE = \sum_{i=1}^n (y_c - y_e)_i^2 \quad (6)$$

3. Results and discussion

3.1. Physio-chemical analysis

3.1.1. Phytoconstituents of *Vigna stipulacea* seed

The total polyphenolic and lignin composition of VS seed extract was determined from the calibration curve of the tannic acid ($0.0015x-0.0091$, $R^2=0.9864$) and alkali lignin ($0.0056x-0.0021$, $R^2=0.09921$), respectively. Furthermore, their corresponding results were expressed as mg/g tannic acid equivalents and mg lignin g^{-1} cell wall. The total polyphenolic composition of VS seed extract was 56.8 mg tannic acid per g extract, whereas their lignin composition was 7.7 mg lignin per g cell wall.

3.1.2. Structural formation of VS-Fe nanoparticles

The phase formation of VS-Fe nanoparticles was detected from their XRD profile, as shown in Figure 2(b). It revealed the characteristic peak corresponding to the Fe^0 formation at $2\theta = 26.09^\circ$ and 45.45° . Similarly, it showed the peaks corresponding to organic matter, i.e., the bioreducing components in the VS seed extract. Therefore, it confirmed that the VS seed extract was vital in reducing Fe^{3+} to Fe^0 formation and has been adsorbed onto its surface. Additionally, it detected the peaks belonging to the Hematite phase (Fe_2O_3) at 30.15° , 40.53° and 57.76° , whereas the Magnetite phase at 35.84° (Gao *et al.* 2016; Jain *et al.* 2021). Hence, it showed that the Fe^0 nanoparticles were formed along with its metal hydroxides. The formation of hydroxides might have occurred due to exposure to atmospheric conditions. The crystalline nature of VS-Fe is determined from Scherrer's formula (Jayalakshmi and Jeyanthi, 2018) (i.e., $d = 0.9\lambda/\beta\cos\theta$). The significant diffraction peaks were used to determine VS-Fe's crystallite size; their average size was estimated to be 30.65 nm. Therefore, the iron particles (VS-Fe) produced

using VS seed extract showed efficacy in forming particles at the nano-scale.

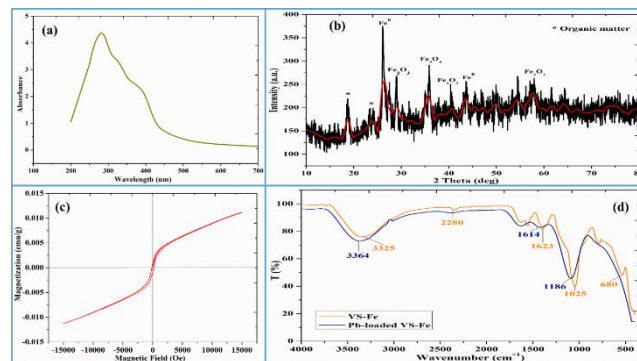


Figure 2. (a) UV-Visible spectra of VS-Fe nanoparticles; (b) XRD diffractogram of VS-Fe nanoparticles; (c) Magnetic hysteresis loop of VS-Fe nanoparticles; (d) IR spectra of VS-Fe and Pb-loaded VS-Fe nanoparticles

To corroborate the bioreducing components that are responsible for VS-Fe formation, the FTIR analysis was performed. The IR spectra of the same were illustrated in Figure 2(d). It showed significant peaks at 3325 cm^{-1} (O-H stretching), 2280 cm^{-1} ($C\equiv C$), 1623 cm^{-1} ($C=C$ ring stretching), 1025 cm^{-1} ($C=O$ stretching) and 680 cm^{-1} ($Fe-O$ stretching) (Lin *et al.* 2020; Ardakani *et al.* 2021). Therefore, these results confirmed the presence of polyphenols (3325 cm^{-1}), lignin content (1623 cm^{-1}) and cellulose content (1025 cm^{-1}) in the surface of VS-Fe synthesized using VS seed extract. Consequently, these bioreducing components might have reduced Fe^{3+} to Fe^0 formation (Eslami *et al.* 2018; Jain *et al.* 2021). Moreover, the presence of metal hydroxides of Fe ions was consistent with the XRD results. Therefore, the formation of these hydroxides might have occurred due to their exposure to air during the characterization. Generally, these hydroxides tend to form a core-shell structure over the VS-Fe's surface (Ardakani *et al.* 2021). The formation of zero-valent iron nanoparticles was further confirmed with the FTIR results. Furthermore, the FTIR result of VS-Fe thus obtained was reliable with the previously reported studies on Fe nanoparticle formation using various plant extracts (Huang *et al.* 2014; Jain *et al.* 2021). The FTIR analysis of Pb-loaded VS-Fe was depicted in Figure 2(d), exhibiting the absence of a peak associated with the alkane and metal oxide functional group. In addition, alterations of peaks were observed at 3325 , 1614 and 1186 cm^{-1} , suggesting the alterations caused by Pb^{2+} ion uptake onto VS-Fe. This furthered the confirmation of the occurrence of chemisorption in Pb^{2+} adsorption utilizing VS-Fe.

To detect the magnetic properties of VS-Fe nanoparticles, the VSM analysis was performed. Figure 2(c) represents the magnetic hysteresis loop of VS-Fe nanoparticles from which their magnetic saturation and coercivity can be estimated. It further revealed the ferromagnetic behavior of VS-Fe nanoparticles, confirming their magnetization function when exposed to an external magnetic field. The estimated VS-Fe's magnetic saturation (M_s) and coercivity (H_c) were found to be 11.21 m emu and 156.65 Oe, respectively. The low magnetic saturation of VS-Fe that hindered their magnetic property might be due to either of

the following reasons: their exposure to air or higher concentration of bioreducing agent in it (Kianpour *et al.* 2017; Kheshtzar *et al.* 2019). Moreover, it showed magnetic remittance (M_r) of 877.73 μ emu. The VSM results showed better magnetic saturation when compared to that reported by Ardakani *et al.* (2021). The report presented the zero magnetic saturation (i.e., no hysteresis loop) of Fe nanoparticles synthesized using *Chlorophytum comosum* leaf extract. Therefore, the compelling magnetic nature of VS-Fe facilitates the magnetic separation after the Pb^{2+} adsorption process.

To get insightful surface area distribution of VS-Fe nanoparticles, it was further analyzed with BET surface area analysis. From the N_2 adsorption/desorption curve isotherm, as displayed in Figure 3(a), the BET plot (not shown here) and BJH plot (insert image) was drawn to estimate surface area and pore distribution. It revealed the Type IV isotherm curve with an H_3 hysteresis loop (Keluo *et al.* 2018), signifying the groove-shaped pores (i.e., parallel plate-shaped pores) comprising mesopores (Mahmoud *et al.* 2021). The surface area of VS-Fe was 199.189 m^2/g which is higher when compared to the one synthesized using various plant extracts (Fazlzadeh *et al.* 2017; Bounab *et al.* 2021). The average pore radius of VS-Fe was 15.50 \AA , whereas their total pore volume was 0.365 cm^3/g . The pore distribution of VS-Fe (Figure 3(a) insert image) revealed that the pores were distributed in the range of 10 – 20 \AA and 50 – 100 \AA . The VS-Fe nanoparticles yielded good surface area characteristics, i.e., higher surface area with mesoporous structure, which are good enough to efficiently uptake Pb^{2+} ions.

To validate the effectiveness of VS-Fe nanoparticles for Pb^{2+} uptake, their net surface charges (i.e., point of zero charge, pH_{pzc}) were further assessed with the salt-addition method (Sulaiman and Al-Jabari, 2021). For this purpose, the VS-Fe nanoparticles were immersed in 0.01 M $NaNO_3$ solution that was adjusted to various pH (pH_i) and was agitated constantly (150 rpm) for 24 hr in an orbital shaker. Subsequently, the suspension's final pH (pH_f) was noted. The pH_{pzc} of VS-Fe was obtained from the plot of (pH_i) vs. ΔpH ($pH_f - pH_i$) as represented in Figure 3(b). And the pH_{pzc} of VS-Fe nanoparticles was 7.2, signifying that the net surface charges on their surface will be positive below its pH_{pzc} , whereas above pH_{pzc} , it is negative. Moreover, the zeta potential analysis (graph not shown here) exhibited -17.9 mV, showing their relative stability in the aqueous medium.

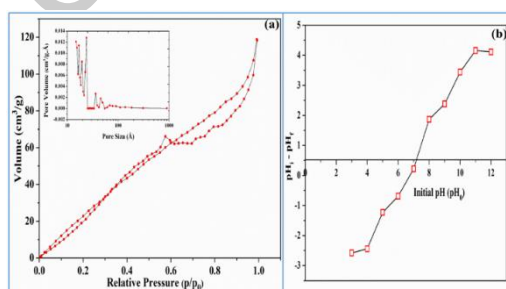


Figure 3. (a) N_2 adsorption/desorption curve and BJH plot (insert image) of VS-Fe nanoparticles; (b) Plot of pH_{pzc} of VS-Fe nanoparticles

3.1.3. Morphology of VS-Fe nanoparticles

The surface texture and morphology of VS-Fe were visualized from their SEM micrograph, as presented in Figure 4(a). The as-synthesized VS-Fe nanoparticles were found to be spherical-shaped particles uniformly distributed with lesser agglomeration. The phytochemicals that are present in the VS seed extract are attributed to agglomeration (Wu *et al.* 2015; Mahmoud *et al.* 2021). Some literature has also reported that the Fe ions' magnetic interaction might have caused the agglomeration (Fazlzadeh *et al.* 2017; Katata-Seru *et al.* 2018). Further, the surface texture of VS-Fe after the adsorption of Pb^{2+} was displayed in Figure 4(b). The particles of Pb-loaded VS-Fe showed non-uniformity in their distribution, i.e., different-sized particles. The observed variations in size following the Pb^{2+} adsorption may be attributed to the development of aggregates. As a result of aggregate formation, the surface texture of the VS-Fe nanoparticles has exhibited roughness. The aggregation of VS-Fe after the Pb^{2+} uptake determined the chemical bond formed between the Pb^{2+} ions and VS-Fe's surface particles. Thus, revealing the occurrence of chemisorption that was further assessed with kinetic studies.

To detect the element composition present in the as-synthesized VS-Fe nanoparticles, the EDAX analysis (Figure 4(c)) was performed. It affirmed the characteristic peaks for Iron (Fe), thus confirming the existence of Fe in VS-Fe nanoparticles. Furthermore, the presence of Oxygen (O) revealed the formation of Fe metal oxides/hydroxides (Kumar *et al.* 2013) that are consistent with the XRD and FTIR results. Moreover, the appearance of Carbon (C) and Oxygen (O) is attributed to the presence of phytochemicals in VS seed extract. Thus, confirming the existence of VS seed extract's coating on their surface (Sraavanthi *et al.* 2018). Furthermore, the presence of Chlorine (Cl) was found as a result of residue formation during the synthesis of VS-Fe nanoparticles.

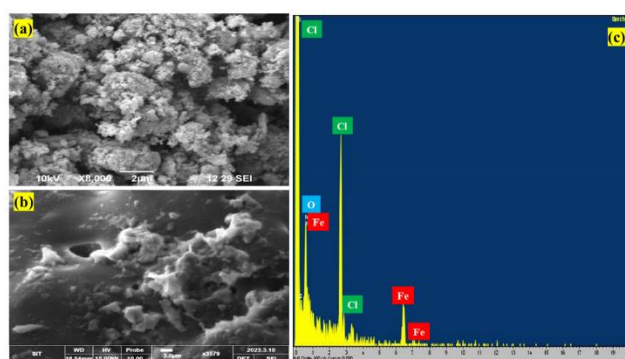


Figure 4. SEM micrograph of VS-Fe nanoparticles before (a) and after (b) Pb^{2+} adsorption; (c) EDAX analysis of VS-Fe nanoparticles

3.2. Removal of Pb^{2+} ions using VS-Fe nanoparticles

3.2.1. Influence of VS-Fe dosage

The quantity of adsorbent utilized for the metal adsorption process is a critical parameter determining the adsorption capacity (Jayalakshmi *et al.* 2022). Initially, the batch experiments were conducted by varying the VS-Fe dosage as follows: 0.01, 0.03, 0.05, 0.07 and 0.10 g/ 100 mL. The

varying dosage of VS-Fe was added into various Erlenmeyer flasks that contained 100 mL of 25 mg/L Pb^{2+} solution and were agitated at 150 rpm under room temperature. The pH of the Pb^{2+} solution was maintained at 6. The influence of VS-Fe dosage on Pb^{2+} uptake was illustrated in Figure 5(a). The Pb^{2+} uptake showed a rapid uprising on adding 0.01 g/ 100 mL of VS-Fe, showing 90.5% removal efficiency. However, upon further increasing the VS-Fe dosage (0.01–0.10 g/ 100 mL), the Pb^{2+} removal efficiency decreased from 90.5 to 50.25%. The downfall in Pb^{2+} uptake may be due to the overcrowding of VS-Fe's binding sites with the reduced surface area on further inclined VS-Fe dosage (Pal *et al.* 2017). Therefore, 0.01 g/ 100 mL VS-Fe was fixed as the optimum dosage for further experiments.

3.2.2. Influence of Pb^{2+} solution pH

The adsorption capability is notably influenced by variations in the pH of the solution, as this leads to modifications in the activity of the surface-active sites. Therefore, the influence of pH on the Pb^{2+} uptake was examined by agitating 0.01 g VS-Fe with 100 mL lead solution at varied pH ranging from 3 to 10. Figure 5(b) represents the effect of pH on the Pb^{2+} uptake using VS-Fe.

The efficacy of Pb^{2+} elimination exhibited an incremental trend until pH 6 (Figure 5(b)), followed by a gradual decline at elevated pH levels (i.e., above pH 6). At a pH greater than 6, the precipitation of lead ions occurs in the form of $Pb(OH)_2$ (Bektas *et al.* 2004). This process results in a decrease in the rate of lead adsorption, ultimately leading to a reduction in lead removal efficiency (Luo *et al.* 2013; Li *et al.* 2017). Therefore, the Pb^{2+} removal efficiency achieved at pH 6 was 96.7 %. The results are consistent with the studies reported by Lakkaboyana *et al.* (2021) and Shi *et al.* (2022). Moreover, the generation of a highly porous layer of iron oxides (Fe-OH) and hydroxides (Fe-O-OH) is facilitated by an increase in pH (6.0), which in turn promotes the diffusion process of the elements towards the Fe^0 core. Consequently, the sorption capacity of the VS-Fe nanoparticles is enhanced (Azzam *et al.* 2016).

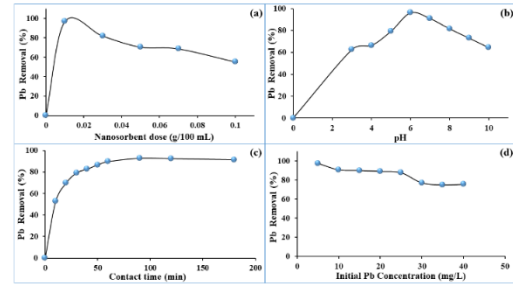


Figure 5. Batch optimization studies on Pb^{2+} adsorption onto VS-Fe, Influence of (a) VS-Fe dosage; (b) pH of lead solution; (c) Contact time; (d) Initial Pb concentration

3.2.3. Influence of contact time (CT)

The CT is a significant parameter that determines the designing of the adsorbent cost. The impact of contact time on Pb^{2+} uptake using VS-Fe was performed by varying the CT to 10 to 180 min. A 0.01 g/ 100 mL VS-Fe was added to 25 mg/L Pb^{2+} solution and it was agitated at 150 rpm with 6 pH under room temperature. The influence of CT on Pb^{2+} removal using VS-Fe is shown in Figure 5(c). It revealed that the Pb^{2+} uptake showed a rapid increase upto 60 min and exhibited no significant change after 60 min, thus confirming their equilibrium attainment. During the initial period of adsorption (10 – 60 min), the Pb^{2+} ions might have engaged quickly onto the binding sites on the VS-Fe's surface, resulting in rapid Pb^{2+} removal. Thus, the Pb^{2+} removal efficiency increased from 11.83% to 96.7%. Over a period of time, active surface sites get exhausted and the Pb^{2+} uptake remains constant due to the unavailability of active sites. Consequently, the VS-Fe showed equilibrium attainment during 70 min with a removal efficiency of 96.82%. Moreover, the VS-Fe possessed 240.24 mg/g adsorption capacity at 60 min. Therefore, further experiments were performed with 60 min of contact time as optimal contact time.

To reveal the rate of Pb^{2+} adsorption and its mechanism, adsorption kinetic modeling was assessed through a non-linear regression approach, as mentioned in Eq. (7) – (9).

$$q_t = q_e \left(1 - e^{-k_1 t}\right) \quad \text{Pseudo-first-order} \quad (\text{Balasubramanian et al. 2021}) \quad (7)$$

where q_t is the adsorption capability of VS-Fe at any time and k_1 is pseudo-first-order rate constant

$$q_t = \frac{k_2 q_e^2 t}{1 + k_2 q_e t} \quad \text{Pseudo-second-order} \quad (\text{Balasubramanian et al. 2021}) \quad (8)$$

where q_e is the adsorption capability of VS-Fe and k_2 is pseudo-second-order rate constant

$$q_t = \left(\frac{1}{\beta}\right) \ln \alpha \beta t \quad \text{Elovich model} \quad (\text{Balasubramanian et al. 2021}) \quad (9)$$

where α is the initial Pb^{2+} adsorption rate and β is the desorption constant.

The corresponding kinetic parameters were obtained directly from the fit of q_t vs. t (plot not shown here) and respective values are tabulated (Table 1).

Based on the higher R^2 values and least EF values (Table 1), the best fit kinetic model for Pb^{2+} adsorption onto VS-Fe was ordered hierarchically as follows: pseudo-second order, pseudo-first order and Elovich model. Consequently, the higher R^2 values (0.9903) and least EF values (RMSE =

3.3401; $\chi^2 = 0.4646$; SSE = 68.90) of pseudo-second-order is said to provide good fitness to Pb^{2+} uptake using VS-Fe. Moreover, the $q_{e(\text{exp})}$ value (240.24 mg/g) obtained for Pb^{2+} is consistent with $q_{e(\text{cal})}$ value (248.61 mg/g) determined from pseudo-second-order. Hence, it further confirmed the best fitness of pseudo-second-order for the Pb^{2+} adsorption using VS-Fe nanoparticles. Thus, concluding the governance of chemisorption. Although the Elovich model

provided lower R^2 values and higher EF values, their $q_{e(cal)}$ (235.64 mg/g), value showed consistency with $q_{e(exp)}$ value (240.24 mg/g). Thus, suggesting their fitness for Pb^{2+} adsorption using VS-Fe. Furthermore, their lower β value further corroborated the chemisorptive behavior of Pb^{2+} removal using VS-Fe nanoparticles.

3.2.4. Influence of initial Pb^{2+} ion concentration

The mass transfer resistance required for Pb^{2+} to pass through the VS-Fe's surface from their metal solution can be significantly influenced by their initial Pb^{2+} ion concentration (Balasubramanian *et al.* 2021). The influence of initial Pb^{2+} ion concentration (C_0) is evaluated by varying their concentration from 5–50 mg/L and the corresponding experiment was carried out under optimized conditions (CT = 60 min; VS-Fe dos = 0.01 g/ 100 mL; pH = 6). The influence of Pb^{2+} ion concentration on Pb^{2+} uptake using VS-Fe was illustrated in Figure 5(d). As it is noticed from Figure 5(d), the Pb^{2+} removal efficiency showed a declining trend with increased C_0 values. On the contrary, the VS-Fe's adsorption capacity increased from 48.70 mg/g to 302.25 mg/g with elevated C_0 values from 5 mg/l to 50 mg/L. The metal ions get adsorbed rapidly onto the VS-Fe's surface at their lower concentration, thereby contributing to the

maximum Pb^{2+} removal efficiency. These binding sites on the VS-Fe get accommodated over the uprising concentration of Pb^{2+} ions and become insufficient to hold up more Pb^{2+} ions, resulting in decreased Pb^{2+} removal efficiency (Jayalakshmi *et al.* 2022).

Table 1. Parameters estimated from Non-linear kinetic models

Pseudo-first order model
$q_{e(cal)} = 225.71 \text{ mg/g}$, $k_1 = 0.0769 \text{ (min}^{-1}\text{)}$, $R^2 = 0.9517$, $RMSE = 7.4785$, $\chi^2 = 2.4492$, $SSE = 149.48$
Pseudo-second order model
$q_{e(cal)} = 248.61 \text{ mg/g}$, $k_2 = 0.0004 \text{ (g/mg/min)}$, $R^2 = 0.9903$, $RMSE = 3.3401$, $\chi^2 = 0.4646$, $SSE = 68.90$
Elovich model
$q_{e(cal)} = 235.64 \text{ mg/g}$, $\alpha = 294.90$, $\beta = 0.0295$, $R^2 = 0.8918$, $RMSE = 11.196$, $\chi^2 = 5.4461$, $SSE = 78.603$

To get insight into the details of VS-Fe's surface properties and their affinity towards Pb^{2+} ions, the adsorption isotherm modeling was assessed through a non-linear regression approach. The following isotherm models, as mentioned in Eq. (10), (12), (13) and (14), were used to establish the correlation between Pb^{2+} concentration and VS-Fe nanoparticles.

$$q_e = q_{\max} \frac{K_L C_e}{1 + K_L C_e} \quad \text{Langmuir isotherm} \quad (10)$$

where q_{\max} is maximum adsorption capacity (Balasubramanian *et al.* 2021), K_L is Pb^{2+} adsorption constant's free energy (Balasubramanian *et al.* 2021)

$$R_L = \frac{1}{1 + K_L C_0} \quad \text{Separation factor (dimensionless)} \quad (11)$$

$$q_e = K_F C_e^{1/n_F} \quad \text{Freundlich isotherm} \quad (12)$$

where K_F is VS-Fe's relative adsorption capacity, $1/n_F$ is Pb^{2+} adsorption intensity constant

$$q_e = \frac{RT}{b} \ln(K_T C_e) \quad \text{Temkin isotherm} \quad (13)$$

where K_T is Temkin constant, b is the intensity of Pb^{2+} adsorption constant, R is the universal gas constant, T is the temperature (K) (Balasubramanian *et al.* 2021)

$$q_e = q_s \exp(\beta_D \varepsilon^2) \quad \text{Dubinin-Radushkevich (D-R) isotherm} \quad (14)$$

$$\varepsilon = RT \ln \left(1 + \frac{1}{C_e} \right) \quad \text{Polanyi potential (Jayalakshmi and Jeyanthi, 2019)} \quad (15)$$

where q_s is saturation capacity (theoretical) and β_D is D-R isotherm constant

The corresponding kinetic parameters were obtained directly from the fit of q_e vs. C_e (plot not shown here). Table 2 presents the values of isotherm model parameters, R^2 and EF.

Based on the higher R^2 and lower EF values (Table 2), the best-fit isotherm model for Pb^{2+} adsorption onto VS-Fe was ordered as follows: Langmuir isotherm > Freundlich isotherm > D-R isotherm. The results from Table 2 also revealed that Temkin isotherm gave a poor fit for Pb^{2+} uptake due to the most negligible R^2 value and higher EF value. The Langmuir isotherm showed a q_{\max} of 1020.50 mg/g for Pb^{2+} adsorption using VS-Fe. Moreover, Langmuir isotherm's suitability was further confirmed with the R_L value (0.796), showing values within 0 and 1. Therefore, the findings showed the favourability of Langmuir isotherm. Likewise, the Freundlich isotherm's favourability on Pb^{2+} adsorption was confirmed with its heterogeneity factor (n_F

= 1.1980), showing values greater than 1. Thus, revealing the surface heterogeneity of VS-Fe, thereby exposing their chemisorptive behavior on Pb^{2+} uptake. These results are consistent with SEM results (Figure 4(b)). All these established findings substantiate that both monolayer and multilayer adsorption co-occurring governed the Pb^{2+} adsorption using VS-Fe. Moreover, it showed that the Pb^{2+} adsorption using VS-Fe might be driven by one or more forces of attraction.

3.3. Mass transfer modeling for Pb^{2+} adsorption onto VS-Fe

To predict the rate-controlling step and mass transfer of Pb^{2+} ions onto VS-Fe's surface, mass transfer modeling was assessed through a linear regression approach. The following diffusion models, as mentioned in the following Eq. (16) and (17), were used to examine the transport of Pb^{2+} ions from their solution onto the VS-Fe's surface.

Where k_{id} and k_{fd} represent the diffusion constants of the intraparticle and liquid film model, respectively, C_i denotes the boundary layer thickness between the Pb^{2+} and VS-Fe.

$$q_t = k_{id}t^{0.5} + C_i \quad \text{Intraparticle diffusion} \quad (16)$$

$$\ln(1-F) = -k_{fd}t + C_{fd} \quad \text{Liquid film diffusion} \quad (17)$$

Table 2. Isotherm parameters for Pb^{2+} adsorption using VS-Fe

Langmuir isotherm	$q_m = 1020.50 \text{ mg/g}$, $K_L = 0.0102 \text{ L/mg}$, $R_L = 0.796$ $R^2 = 0.9941$, RMSE = 7.2075, $\chi^2 = 1.4966$, SSE = 3.0169
Freundlich isotherm	$n_F = 1.1980$, $K_F = 14.667 \text{ L/mg}$ $R^2 = 0.9743$, RMSE = 15.080, $\chi^2 = 6.4003$, SSE = 6193.9
Temkin isotherm	$b = 268.96 \text{ J/mol}$, $K_T = 2.68 \times 10^7 \text{ L/mg}$ $R^2 = 0.13990$, RMSE = 87.238, $\chi^2 = 249.77$, SSE = 372.79
D-R isotherm	$q_s = 297.52 \text{ mg/g}$, $\beta_D = 0.0686 \text{ mol}^2/\text{kJ}^2$ $R^2 = 0.9039$, RMSE = 29.155, $\chi^2 = 2292.24$, SSE = 3150.28

Table 3. Diffusion model parameters for Pb^{2+} removal using VS-Fe

Intraparticle diffusion model	
$k_{id} \text{ (mg/g/min}^{0.5})$	$= 19.441$, $C_i = 80.798$, $R^2 = 0.9419$
Liquid film diffusion model	
$k_{fd} \text{ (min}^{-1})$	$= 0.0607$, $C_{fd} = -0.281$, $R^2 = 0.9904$

The findings derived from Table 3 indicate that the rate-limiting step for removing Pb^{2+} onto VS-Fe cannot be attributed to either intraparticle diffusion or liquid film diffusion. When the respective plots pass through the origin, it has been suggested that either of these models governs the mass transfer mechanism. The linear plot of intraparticle diffusion for the Pb^{2+} removal indicated a departure from the origin, indicating the possibility of surface diffusion in conjunction with intraparticle diffusion (Fang *et al.* 2018; Egbiedina *et al.* 2021). Moreover, the elevated C_i value (80.798) indicates that the adsorption of Pb^{2+} was significantly influenced by the boundary layer, which could have experienced substantial resistance to the external mass transfer (Dubey *et al.* 2015). The present study further assessed the impact of the boundary layer on the Pb^{2+} adsorption by employing the Liquid film diffusion model. Despite the fact that their linear plot did not exhibit a passing through the origin, the minimal values of C_{fd} (-0.281) suggest that the Pb^{2+} adsorption may have been slightly influenced by liquid film diffusion (Wei *et al.* 2016). Therefore, the mass transfer of Pb^{2+} ions onto VS-Fe is influenced by multiple diffusion mechanisms.

3.4. Mechanism/interaction involved in sequestration of Pb^{2+} ions

The possible mechanism/interaction involved in the sequestration of Pb^{2+} ions using VS-Fe nanoparticles may be reduction, electrostatic sorption and precipitation. An increase in pH (6.0) facilitated the formation of a highly porous layer of iron oxides (Fe-OH) and hydroxides (Fe-O-OH), which in turn promoted the diffusion of Pb^{2+} ions towards the Fe^0 core. Hence, the reduction happens during the sequestration of Pb^{2+} ions. Moreover, the high $[H^+]$

The corresponding diffusion constants were obtained from the linear plot of the intraparticle and liquid film diffusion model (not shown here) and are presented in Table 3.

under acidic conditions may impede the absorption of Pb^{2+} ions onto the positively charged VS-Fe surface ($pH < pH_{pzc}$) as a result of electrostatic repulsion. As the pH levels get elevated, the competition among reaction sites will be reduced, leading to enhanced mobility of Pb^{2+} ions towards the negatively charged VS-Fe due to electrostatic attraction. This phenomenon facilitates the efficient removal of Pb^{2+} ions.

Furthermore, the Pb^{2+} ions precipitate in alkaline pH above 6 and form lead hydroxides. Hence, rendering the removal of Pb^{2+} ions through precipitation in alkaline pH (i.e., $pH > 6$). Due to the precipitation nature of lead species in alkaline pH, their optimal pH was set as 6 for their effective sequestration. At this optimal pH, the chemisorption is dominant over physisorption. Additionally, the isotherm and kinetic modeling findings revealed the dominance of chemisorption. These results were further confirmed with the SEM and FTIR analysis of Pb-loaded VS-Fe nanoparticles.

3.5. Comparison studies on VS-Fe's adsorption capability with other adsorbents

Table 4 presents a comparison of various adsorbents utilized for Pb^{2+} adsorption, with a focus on their maximum adsorption capacity. The q_m value for VS-Fe was determined to be 1020.50 mg/g, indicating favorable performance. This value is comparatively more significant than the q_m values reported for other adsorbents in the literature.

Table 4. Comparison of various adsorbents utilized for Pb^{2+} adsorption

Adsorbent	q_m (mg/g)	Reference
Activated carbon-supported nanoscale zero-valent iron composite	59.35	Liu <i>et al.</i> 2019
Kaolin (IK) supported nano zerovalent iron composite	192	Lakkaboyana <i>et al.</i> 2021
Nanoscale zero-valent iron-carbon materials	223.52	Shi <i>et al.</i> 2022
Copper slag-supported sulfidized nanoscale zero-valent iron	338.98	Shi <i>et al.</i> 2023
Carbon@nano-zero-valent iron composite	98.37	Yang <i>et al.</i> 2023
Sulfur-modified nanoscale zero-valent iron	246.40	Tang <i>et al.</i> 2023
VS-Fe nanoparticle	1020.50	Present study

3.6. Feasibility of VS-Fe nanoparticles

The synthesis technique of VS-Fe is characterized by its simplicity and cost-effectiveness, as it does not need any

specialized knowledge. The utilization of *Vigna stipulacea* seed extract as a reducing agent is advantageous due to its natural composition, minimal chemical requirement, sustainability and biocompatibility, hence rendering the VS-Fe environmentally beneficial. Moreover, these *Vigna stipulacea* plants are easily domesticated as they require minimal water and demand little care and maintenance. Furthermore, the VS seed extract proved its efficacy in acting as a reducing agent in Fe⁰ nanoparticle formation, confirmed by their instrumental analysis. The key findings are as follows: the UV analysis showed the corresponding surface plasma resonance exhibited in its absorbance peak; the XRD analysis established the crystal size formation in nano-scale; the FTIR analysis showed the presence of polyphenols and lignin content; the EDAX analysis confirmed the existence of Fe species.

Additionally, the VS-Fe exhibited a greater surface area, resulting in an increased adsorption capacity. Moreover, it established adequate magnetic saturation, thereby facilitating the separation process using an external magnetic field. The non-functionalized VS-Fe exhibited a maximum adsorption capacity compared to other functionalized nano-iron. However, for long-term applications, the stability of VS-Fe could still be improved by functionally it with polymer to overcome the reduction in electron transfer issues caused by the surface passivation.

The regeneration capacity of VS-Fe (not reported here) may be easily achieved for up to three cycles, resulting in a maximum removal effectiveness of 95%. It has the potential to decrease the expenses associated with wastewater treatment significantly. The dominance of chemisorption might attributed to the reduction in VS-Fe's regeneration capacity after the third cycle. However, for long-term applications, the capability of VS-Fe could still be improvised in future applications to reuse it more efficiently.

4. Conclusion

The present investigation focused on utilizing *Vigna stipulacea*'s seed extract for synthesizing Fe nanoparticles and reported their capability of eliminating Pb²⁺ ions from an aqueous environment. The UV-Vis analysis confirmed the surface plasmon resonance spectra (285 nm) for VS-Fe nanoparticles' formation. In addition, a spherical shape with less agglomeration and uniform size distribution of VS-Fe was observed from SEM analysis. Moreover, the FTIR analysis showed the peaks associated with polyphenols and other phytochemicals, which played a crucial role in VS-Fe's bioreduction and stabilization. Batch adsorption studies on VS-Fe indicated maximum Pb²⁺ removal (96.7%) was achieved within 60 min using 0.01 g/ 100 mL dosage at pH 6. The Pb²⁺ adsorption using VS-Fe indicated a reasonable fit to Langmuir and Freundlich isotherm models. Moreover, the Langmuir isotherm showed a monolayer adsorption capacity of 1020.50 mg/g.

Similarly, the Pb²⁺ adsorption kinetics showed better fitness with pseudo-second-order and the Elovich model. Furthermore, it indicated the dominance of chemisorption

in Pb²⁺ removal. The experimental findings suggest that VS-Fe nanoparticles have the potential to serve as effective adsorbents to eliminate Pb²⁺ ions from wastewater. Moreover, it facilitates the development of a cost-effective wastewater treatment system to eliminate hazardous metals, thereby mitigating the adverse impacts on water quality. Thus, it can be inferred that the combined strategy of nanotechnology and a greener approach can be utilized for wastewater treatment, which in turn creates a new frontier in environmental pollution.

Acknowledgment

The authors express their gratitude to Principal and Management of Coimbatore Institute of Technology, Coimbatore, for providing the required lab facilities.

References

- Ali H., Khan E. and Ilahi I. (2019). Environmental chemistry and ecotoxicology of hazardous heavy metals: environmental persistence, toxicity, and bioaccumulation, *Journal of chemistry*, **2019**.
- Araújo C. S., Almeida I. L., Rezende H. C., Marcionilio S. M., Léon J. J. and de Matos T. N. (2018). Elucidation of mechanism involved in adsorption of Pb (II) onto lobeira fruit (*Solanum lycocarpum*) using Langmuir, Freundlich and Temkin isotherms, *Microchemical Journal*, **137**, 348–354.
- Ardakani L. S., Alimardani V., Tamaddon A. M., Amani A. M. and Taghizadeh S. (2021). Green synthesis of iron-based nanoparticles using *Chlorophytum comosum* leaf extract: methyl orange dye degradation and antimicrobial properties, *Heliyon*, **7(2)**, e06159.
- Azzam A. M., El-Wakeel S. T., Mostafa B. B. and El-Shahat M. F. (2016). Removal of Pb, Cd, Cu and Ni from aqueous solution using nano scale zero valent iron particles, *Journal of environmental chemical engineering*, **4(2)**, 2196–2206.
- Balasubramanian U. M., Vaiyazhipalayam Murugaiyan S. and Marimuthu T. (2021). Sustainable robust green synthesis of nanoparticles from waste aquatic plants and its application in environmental remediation, *Water Science and Technology*, **84(12)**, 3599–3615.
- Bektaş N., Ağim B. A. and Kara S. (2004). Kinetic and equilibrium studies in removing lead ions from aqueous solutions by natural sepiolite, *Journal of Hazardous materials*, **112(1–2)**, 115–122.
- Bounab N., Duclaux L., Reinert L., Oumedjbeur A., Boukhalfa C., Penhoud P. and Muller F. (2021). Improvement of zero valent iron nanoparticles by ultrasound-assisted synthesis, study of Cr (VI) removal and application for the treatment of metal surface processing wastewater, *Journal of Environmental Chemical Engineering*, **9(1)**, 104773.
- Dayanidhi K., Vadivel P., Jothi S. and Eusuff N. S. (2020). Facile synthesis of Silver@ Eggshell nanocomposite: A heterogeneous catalyst for the removal of heavy metal ions, toxic dyes and microbial contaminants from water, *Journal of Environmental Management*, **271**, 110962.
- Ding Y., Wu J., Wang J., Wang J., Ye J. and Liu F. (2020). Superhydrophilic carbonaceous-silver nanofibrous membrane for complex oil/water separation and removal of heavy metal ions, organic dyes and bacteria, *Journal of membrane science*, **614**, 118491.
- Dong Q., Guo X., Huang X., Liu L., Tallon R., Taylor B. and Chen J. (2019). Selective removal of lead ions through capacitive

- deionization: Role of ion-exchange membrane, *Chemical Engineering Journal*, **361**, 1535–1542.
- Dubey R., Bajpai J. and Bajpai A. K. (2015). Green synthesis of graphene sand composite (GSC) as novel adsorbent for efficient removal of Cr (VI) ions from aqueous solution. *Journal of water process engineering*, **5**, 83–94.
- Ebrahiminezhad A., Zare-Hoseinabadi A., Sarmah A. K., Taghizadeh S., Ghasemi Y. and Berenjian A. (2018). Plant-mediated synthesis and applications of iron nanoparticles. *Molecular biotechnology*, **60**, 154–168.
- Egbedina A. O., Adebawale K. O., Olu-Owolabi B. I., Unuabonah E. I. and Adesina M. O. (2021). Green synthesis of ZnO coated hybrid biochar for the synchronous removal of ciprofloxacin and tetracycline in wastewater, *RSC advances*, **11(30)**, 18483–18492.
- El-Hosiny F. I., Abdel-Khalek M. A., Selim K. A. and Osama I. (2018). Physicochemical study of dye removal using electro-coagulation-flotation process, *Physicochemical problems of mineral processing*, **54(2)**, 321–333.
- Eslami S., Ebrahimzadeh M. A. and Biparva P. (2018). Green synthesis of safe zero valent iron nanoparticles by Myrtus communis leaf extract as an effective agent for reducing excessive iron in iron-overloaded mice, a thalassemia model, *RSC advances*, **8(46)**, 26144–26155.
- Fang L., Xu X., Li J., Zheng F., Li M., Yan J. and Zeng S. (2020). Transcriptome analysis provides insights into the non-methylated lignin synthesis in Paphiopedilum armeniacum seed, *BMC genomics*, **21(1)**, 1–15.
- Fang Z., Hu Y., Wu X., Qin Y., Cheng J., Chen Y. and Li H. (2018). A novel magnesium ascorbyl phosphate graphene-based monolith and its superior adsorption capability for bisphenol A, *Chemical Engineering Journal*, **334**, 948–956.
- Fazlzadeh M., Rahmani K., Zarei A., Abdoallahzadeh H., Nasiri F. and Khosravi, R. (2017). A novel green synthesis of zero valent iron nanoparticles (NZVI) using three plant extracts and their efficient application for removal of Cr (VI) from aqueous solutions, *Advanced Powder Technology*, **28(1)**, 122–130.
- Gao J. F., Li H. Y., Pan K. L. and Si C. Y. (2016). Green synthesis of nanoscale zero-valent iron using a grape seed extract as a stabilizing agent and the application for quick decolorization of azo and anthraquinone dyes, *RSC advances* **6(27)**, 22526–22537.
- Guo M., Weng X., Wang T. and Chen Z. (2017). Biosynthesized iron-based nanoparticles used as a heterogeneous catalyst for the removal of 2, 4-dichlorophenol, *Separation and Purification Technology*, **175**, 222–228.
- Harouna D. V., Venkataramana P. B., Ndakidemi P. A. and Matemu A. O. (2018). Under-exploited wild Vigna species potentials in human and animal nutrition: A review, *Global food security*, **18**, 1–11.
- Huang L., Weng X., Chen Z., Megharaj M. and Naidu R. (2014). Synthesis of iron-based nanoparticles using oolong tea extract for the degradation of malachite green, *Spectrochimica Acta Part A: Molecular and Biomolecular Spectroscopy*, **117**, 801–804.
- Jain R., Mendiratta S., Kumar L. and Srivastava A. (2021). Green synthesis of iron nanoparticles using Artocarpus heterophyllus peel extract and their application as a heterogeneous Fenton-like catalyst for the degradation of Fuchsin Basic dye, *Current Research in Green and Sustainable Chemistry*, **4**, 100086.
- Jayalakshmi R. and Jeyanthi J. (2018). Synthesis and structural characterization of polymer-based cobalt ferrite nanocomposite with core-shell structure, *Journal of Inorganic and Organometallic Polymers and Materials*, **28**, 1286–1293.
- Jayalakshmi R. and Jeyanthi J. (2019). Simultaneous removal of binary dye from textile effluent using cobalt ferrite-alginate nanocomposite: Performance and mechanism, *Microchemical Journal*, **145**, 791–800.
- Jayalakshmi R. and Jeyanthi J. (2021). Dynamic modelling of Alginate-Cobalt ferrite nanocomposite for removal of binary dyes from textile effluent, *Journal of Environmental Chemical Engineering*, **9(1)**, 104924.
- Jayalakshmi R., Jeyanthi J. and Sidhaarth K. A. (2022). Versatile application of cobalt ferrite nanoparticles for the removal of heavy metals and dyes from aqueous solution, *Environmental Nanotechnology, Monitoring and Management*, **17**, 100659.
- Kaur M., Ubhi M. K. and Singh D. (2018). Magnetically retrievable nanocomposite of magnesium ferrite and bentonite clay for sequestration of Pb (II) and Ni (II) ions: a comparative study, *Bulletin of Materials Science*, **41**, 1–14.
- Keluo C. H. E. N., Zhang T., Xiaohui C. H. E. N., Yingjie H. E. and LIANG X. (2018). Model construction of micro-pores in shale: A case study of Silurian Longmaxi Formation shale in Dianqianbei area, SW China, *Petroleum Exploration and Development*, **45(3)**, 412–421.
- Khatun S. and Kim T. (2021). Phenolic compound, antioxidant activity and nutritional components of five legume seed, *American Journal of Biomedical Science and Research*, **12**, 328–334.
- Kheshtzar R., Berenjian A., Ganji N., Taghizadeh S. M., Maleki M., Taghizadeh S. and Ebrahiminezhad A. (2019). Response surface methodology and reaction optimization to product zero-valent iron nanoparticles for organic pollutant remediation, *Biocatalysis and Agricultural Biotechnology*, **21**, 101329.
- Kianpour S., Ebrahiminezhad A., Mohkam M., Tamaddon A. M., Dehshahri A., Heidari R. and Ghasemi Y. (2017). Physicochemical and biological characteristics of the nanostructured polysaccharide-iron hydrogel produced by microorganism Klebsiella oxytoca, *Journal of basic microbiology*, **57(2)**, 132–140.
- Lakkaboyana S. K., Khantong S., Asmel N. K., Obaidullah S., Kumar, V., Kannan K. and Yaacob W. Z. W. (2021). Indonesian Kaolin supported nZVI (IK-nZVI) used for the an efficient removal of Pb (II) from aqueous solutions: Kinetics, thermodynamics and mechanism, *Journal of Environmental Chemical Engineering*, **9(6)**, 106483.
- Li B., Yang L., Wang C. Q., Zhang Q. P., Liu Q. C., Li Y. D. and Xiao R. (2017). Adsorption of Cd (II) from aqueous solutions by rape straw biochar derived from different modification processes. *Chemosphere*, **175**, 332–340.
- Lin Z., Weng X., Owens G. and Chen Z. (2020). Simultaneous removal of Pb (II) and rifampicin from wastewater by iron nanoparticles synthesized by a tea extract, *Journal of Cleaner Production*, **242**, 118476.
- Liu X., Lai D. and Wang Y. (2019). Performance of Pb (II) removal by an activated carbon supported nanoscale zero-valent iron composite at ultralow iron content, *Journal of hazardous materials*, **361**, 37–48.
- Luo X., Liu L., Deng F. and Luo S. (2013). Novel ion-imprinted polymer using crown ether as a functional monomer for

- selective removal of Pb (II) ions in real environmental water samples, *Journal of Materials Chemistry A*, **1(28)**, 8280–8286.
- Mahmoud R., Kotp A. A., El-Ela F. I. A., Farghali A. A., Moaty S. A., Zahran H. Y. and Amin R. (2021). Green synthesis of iron nanoparticles of clove and green coffee origin with an in vivo hepatoprotective investigation, *Journal of Environmental Chemical Engineering*, **9(6)**, 106320.
- Mandal S., Pu S., Wang X., Ma H. and Bai Y. (2020). Hierarchical porous structured polysulfide supported nZVI/biochar and efficient immobilization of selenium in the soil, *Science of the Total Environment*, **708**, 134831.
- Mohamed W. A., Mansour M. M. and Salem M. Z. (2019). Lemna gibba and Eichhornia crassipes extracts: Clean alternatives for deacidification, antioxidation and fungicidal treatment of historical paper, *Journal of Cleaner Production*, **219**, 846–855.
- Nithyalakshmi B. and Saraswathi R. (2021). Removal of colorants from wastewater using biochar derived from leaf waste, *Biomass Conversion and Biorefinery*, 1–17.
- Nithyalakshmi B., Saraswathi R. and Praveen S. (2023). Removal of basic fuchsin red dye by turmeric leaf waste biochar: Batch adsorption studies, isotherm kinetics and RSM studies, *Global Nest Journal*, **25(1)**, 17–27.
- Pal P., Syed S. S. and Banat F. (2017). Gelatin-bentonite composite as reusable adsorbent for the removal of lead from aqueous solutions: Kinetic and equilibrium studies, *Journal of water process engineering*, **20**, 40–50.
- Pan Z., Lin Y., Sarkar B., Owens G. and Chen Z. (2020). Green synthesis of iron nanoparticles using red peanut skin extract: Synthesis mechanism, characterization and effect of conditions on chromium removal, *Journal of colloid and interface science*, **558**, 106–114.
- Panzeri D., Guidi Nissim W., Labra M. and Grassi F. (2022). Revisiting the Domestication Process of African Vigna Species (Fabaceae): Background, Perspectives and Challenges, *Plants*, **11(4)**, 532.
- Patil S. A., Kumbhar P. D., Satvekar B. S., Harale N. S., Bhise S. C., Patil S. K. and Anuse M. A. (2022). Adsorption of toxic crystal violet dye from aqueous solution by using waste sugarcane leaf-based activated carbon: isotherm, kinetic and thermodynamic study, *Journal of the Iranian Chemical Society*, **19(7)**, 2891–2906.
- Raman C. D., Sellappa K. and Mkandawire M. (2021). Facile one step green synthesis of iron nanoparticles using grape leaves extract: textile dye decolorization and wastewater treatment, *Water Science and Technology*, **83(9)**, 2242–2258.
- Saleh M., Isik Z., Aktas Y., Arslan H., Yalvac M. and Dizge N. (2021). Green synthesis of zero valent iron nanoparticles using Verbascum thapsus and its Cr (VI) reduction activity, *Bioresource Technology Reports*, **13**, 100637.
- Shi L., Deng Q., Guo L., Du Y., Du D. and Zhang T. C. (2023). Efficient removal of Cd (II), Cu (II), and Pb (II) in aqueous solutions by exhausted copper slag supported sulfidized nanoscale zerovalent iron, *Separation and Purification Technology*, **314**, 123483.
- Shi Y., Cheng X., Wan D., Zhang Z., Chen Z., Han X. and Zhou Q. (2022). The behavior and mechanism of toxic Pb (II) removal by nanoscale zero-valent iron-carbon materials based on the oil refining by-products, *Inorganic Chemistry Communications*, 109588.
- Sivakami M., Renuka R. and Thilagavathi T. (2020). Green synthesis of magnetic nanoparticles via Cinnamomum verum bark extract for biological application, *Journal of Environmental Chemical Engineering*, **8(5)**, 104420.
- Sulaiman S. M. and Al-Jabari M. H. (2021). Enhanced adsorptive removal of diclofenac sodium from aqueous solution by bentonite-supported nanoscale zero-valent iron, *Arab Journal of Basic and Applied Sciences*, **28(1)**, 51–63.
- Tang K., Zhang S., Ren D., Zhang X., Zhang Z. and Zhang X. (2023). Study on the removal of Pb (II) from water by coated sulfur-modified nanoscale zero-valent iron, *Water Science and Technology*, **87(5)**, 1096–1111.
- Thanh D. N., Novák P., Vejpravova J., Vu H. N., Lederer J. and Munshi T. (2018). Removal of copper and nickel from water using nanocomposite of magnetic hydroxyapatite nanorods, *Journal of magnetism and magnetic materials*, **456**, 451–460.
- Thirulogachandar A., Rajeswari M., Ramya S., 2014. Assessment of heavy metals in Gallus and their impacts on human, *International Journal of Scientific and Research Publications*, **4(6)**, 1–8.
- Wei W., Wang Q., Li A., Yang J., Ma F., Pi S. and Wu D. (2016). Biosorption of Pb (II) from aqueous solution by extracellular polymeric substances extracted from Klebsiella sp. J1: Adsorption behavior and mechanism assessment, *Scientific reports*, **6(1)**, 31575.
- Yang L., Jin X., Lin Q., Owens G. and Chen Z. (2023). Enhanced adsorption and reduction of Pb (II) and Zn (II) from mining wastewater by carbon@ nano-zero-valent iron (C@ nZVI) derived from biosynthesis, *Separation and Purification Technology*, 123249.
- Yurekli Y. (2016). Removal of heavy metals in wastewater by using zeolite nano-particles impregnated polysulfone membranes, *Journal of hazardous materials*, **309**, 53–64.